Proceedings of the ASME 2019 38th International Conference on Ocean, Offshore and Arctic Engineering
OMAE2019
June 9-14, 2019, Glasgow, Scotland, UK

OMAE2019-95929

VALIDATION OF HYDRODYNAMIC LOADS ON A LARGE-DIAMETER MONOPILE IN REGULAR WAVES

Fatemeh H. Dadmarzi[1]
Department of Marine Technology
Norwegian University of Science and Technology, NTNU
Trondheim, Norway

Maxime Thys
SINTEF Ocean,
Trondheim, Norway

Erin E. Bachynski
Department of Marine Technology
Norwegian University of Science and Technology, NTNU
Trondheim, Norway

ABSTRACT

Validated hydrodynamic load models for large-diameter support structures are increasingly important as the industry moves towards larger offshore wind turbines. Experiments at 1:50 scale with stiff, vertical, bottom-fixed, extra-large (9m and 11m diameter full-scale) monopiles in steep waves are conducted. The tests are carried out at two water depths, 27 m and 33 m. A range of regular waves, with varying period and amplitude, are used. The first, second, and third harmonics of the total wave loads, where measurements are available, are calculated with different methods. For the first harmonic of the force (and consequently the mudline moment), MacCamy-Fuchs gives the best agreement with experiments, especially for the larger diameter model. For the second harmonic, for the shortest waves the generalized FNV theory and Morison equation overpredict the forces, while for the longest (and largest) waves, the opposite is observed. The third harmonic of the force is generally overpredicted by the calculations.

INTRODUCTION

Motivated by the adverse effects of climate change, and the promising prospect of wind as a renewable energy source, industry is pushing for larger (6-12MW) offshore wind turbines (OWT), which require larger support structures. Large-diameter monopile foundations are considered for shallow and intermediate water depths in an attempt to reduce the levelized cost of energy. However, as structure size increases, the eigenperiods increase and get closer to the primary wave periods (3-5s), making the structure more susceptible to wave loading, including nonlinear wave loads which may result in ringing-type responses. To better estimate the extreme responses, more accurate and validated analysis methods are needed.

Ringing is defined as the transient response of a structure at frequencies much higher than the incident wave [1]. Ringing generally occurs following a high steep wave. On the other hand, the steady-state response to sum-frequency forces is defined as *springing*.

Nonlinear wave loads contributing to ringing have been studied both numerically [1–3], and experimentally [4,5], in particular due to their role in springing and ringing of tension leg and gravity-based platforms. Faltinsen, Newman & Vinje (1995) (FNV) [6] developed analytical models for ringing loads on a fixed circular cylinder in deep water regular waves. Newman (1996) applied and extended the model to irregular waves. Comparing to the deep water, in the intermediate depth the waves contain larger higher harmonics energy and it is likely to influence the nonlinear wave loads [7]. Hence, Kristiansen and Faltinsen (KF, 2017) [8] generalized the FNV theory to finite water depth for regular waves. Due to the importance of nonlinear loads from steep waves in finite water depths for the design of wind turbines, numerical models with better estimations of loads and structural responses are needed and experimental validation should be carried out as well.

The present experimental study is conducted as a part of the WAS-XL project (Wave loads and soil support for extra large monopiles) [9]. The environmental conditions correspond to the North Sea center as provided by [10]. The project's main objective is ensuring reliable analysis through advancement of validated modelling for large diameter bottom fixed offshore wind turbines.

As part of the project, model scale experiments were conducted and compared to simulations based on different numerical methods. Two monopile models, one uniform and one segmented, were subjected to steep waves and the total load and moment was measured. The tests were carried out at two water depths, with a range of regular waves, with varying

[1] Contact author: fatemeh.h.dadmarzi@ntnu.no

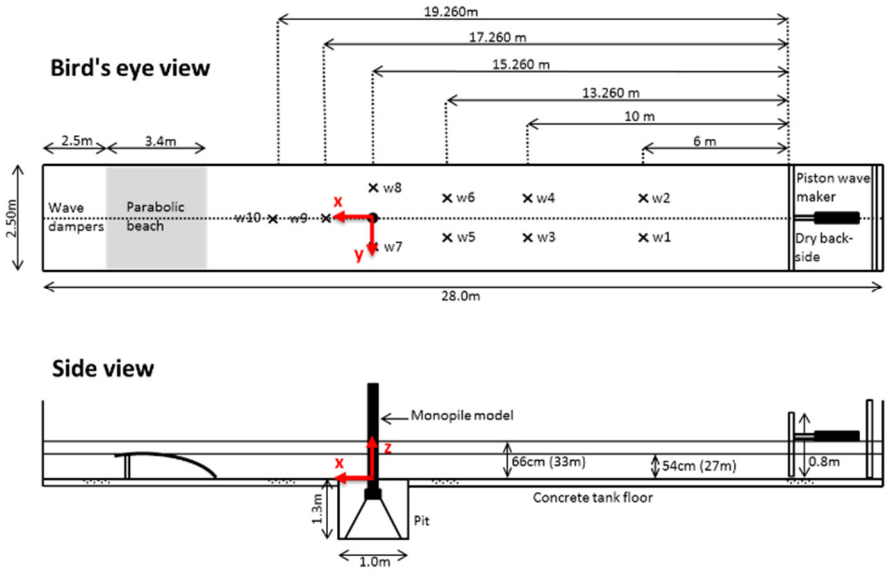

Figure 1: MODEL TEST SETUP, IN MODEL SCALE. SELECTED FULL SCALE VALUES ARE GIVEN IN PARENTHESES.

period and amplitude. The first, second, third, and fourth harmonics of the total wave loads were calculated with MacCamy-Fuchs, KF (generalized FNV) theory and Morison's equation and compared with the measurements.

1. EXPERIMENTAL SETUP

The experiments were conducted in a medium-size tank ('Lilletanken') at the Marine Technology Center in Trondheim, NTNU. The main dimensions of the tank are shown in Figure 1. At one end of the tank, there is a piston-type wavemaker and at the other end, a parabolic beach with adjustable height. In the tests, the upper position of the parabolic beach was 1.5cm (model scale) above the still water line. Based on previous tests [11], the beach reflection is expected to be between 6 to 8%.

Second order correction for regular waves with the piston type wavemaker is adopted in order to avoid generating spurious waves. The tests were performed at two water depths, 27 and 33 m with Froude scale 1:50. All dimensions presented here are in full scale unless stated otherwise. Wave elevations were measured by resistive wave probes. The layout of the wave probes and the model is shown in Figure 1. The calibration of the wave probes was checked daily. The water temperature was recorded and the influence of changes in the water temperature on the conductivity of the wave probes was considered.

Two rigid models with diameters 9m and 11m, here on referred to as Model 1 and 2 respectively, were tested exposed to regular waves. The wave periods (T) of the regular waves are between 6s and 16.5s with step of 0.5s, with steepnesses 1/20, 1/22, 1/25, 1/30, 1/40 (here wave steepness is defined as the first order wave height divided by the wave length). Shear force and bending moment at the base were measured for both models. Model 1 with the diameter of 9m, was segmented in an attempt to measure load distribution along the model. Model 2 with diameter 11m, had uniform shell and only the global force and moments were measured. An accelerometer at the top of both models was used to measure the high frequency accelerations along the wave direction. The sampling rate for measurements was 200Hz with filter at 20Hz (model scale).

In both models, a roughness of 2mm (model scale) induces a turbulent boundary layer similar to full scale. The models have eigenfrequencies above 3.4Hz (24Hz model scale, based on a hammer test after installing the model in the basin) which is approximately 10 times higher than the largest frequencies of interest (around 0.3 Hz for wave period of 10s). Therefore, we consider our model rigid enough for studying loads that excite ringing. Very high-frequency loads due to breaking waves, which can potentially excite the second mode of a full scale turbine [12], are outside of the scope of this study.

Automatic test procedures, similar to the previous studies [11], have been adopted here as well. The wave maker was programmed to run for up to 24 hours. An example of time-series from a 12 hour regular wave test with 122 regular wave conditions is shown in Figure 2. In the tests, a 300s (model scale) pause between each wave condition was used to allow the tank to settle.

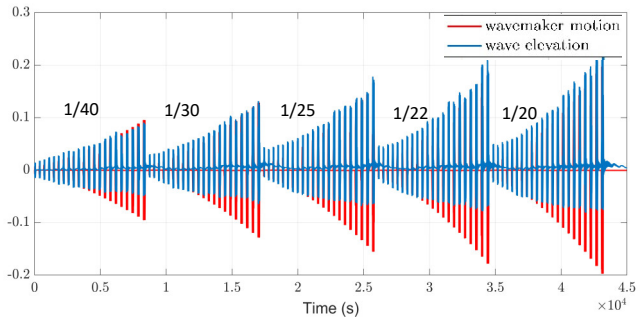

Figure 2: AUTOMATIC TEST PROCEDURE EXAMPLE. RED COLOR SHOWS WAVEMAKER MOTION AND BLUE IS WAVE ELEVATION NEXT TO THE MODEL (WAVE 8). THE WAVE STEEPNESSES ARE SHOWN. VALUES ARE IN MODLE SCALE.

Uncertainty of the experimental results was assessed following the ITTC recommended Procedures and Guidelines[13]. For the uncertainty analysis, only the first harmonic of the global force and moment at mudline were considered as Quantities of Interest (QoIs). According to the ITTC, there are two types of uncertainties, type A obtained based on statistical analysis of a series of observations and type B obtained by other means. Only type B uncertainties were identified since no repetitions of regular wave tests were performed.

The sources of uncertainties considered were related to the model diameter, the water depth, the segmentation on model 1, and the load transducer at mudline. The uncertainty on the diameter was of ± 1.5mm (model scale) for the segmented model and ± 0.5mm for the other model. The water depth was recorded between the tests and the uncertainty was found to be of ± 7 mm (model scale). The influence of the variations in the water depth on the wave height was considered based on wavemaker theory. Model 1 was segmented vertically, with a gap of approximately 1.5 mm (model scale) between each segment. The ratio of the missing volume due to the segmentation over the model volume was multiplied with the load to estimate the uncertainty due to the segmentation. Note that the gap between the segments was considered as an uncertainty and we did not try to correct for the induced error. The uncertainty on the load transducer was derived based on the variation of the load measurements between tests.

The uncertainty on the measured wave elevation was considered as negligible since calibration of wave probes was checked daily. Also, the influence of the temperature on the measured wave elevation was corrected for in the post-processing phase.

The combined uncertainty (u_c) on the QoIs (force and load at mudline) was evaluated by propagating the above-mentioned uncertainties (u_i) for $i = 1$ to N sources of uncertainty,

$$u_c^2 = \sum_{i=1}^{N} c_i^2 u_i^2, \qquad (1)$$

where c_i is the sensitivity coefficient that was computed numerically based on Morison theory and Airy waves and the input quantities were assumed uncorrelated. The combined uncertainty was then multiplied by a coverage factor ($k = 2$), to obtain the expanded uncertainty (U_c^{95}) with a coverage factor of 95%. The experimental results are shown hereafter with error bars indicating the expanded range of uncertainty $\pm U_c^{95}$. Only uncertainty on the first harmonic was considered and the main sources of uncertainty for the higher harmonics can be different.

The square of the standard uncertainties ($c_i^2 u_i^2$) for the global force measured at mudline are shown in Figure 3 for the two models and for two different wave steepness (1/20 and 1/40), for a water depth of 27m. In general, the uncertainty due to the water depth is dominant. Uncertainties on model 2 are in larger than for model 1 due to the larger loads. The change in trend of the standard uncertainty due to the depth, for period above 11s, is due to the use of wavemaker theory to propagate the uncertainty from the water depth to the wave height.

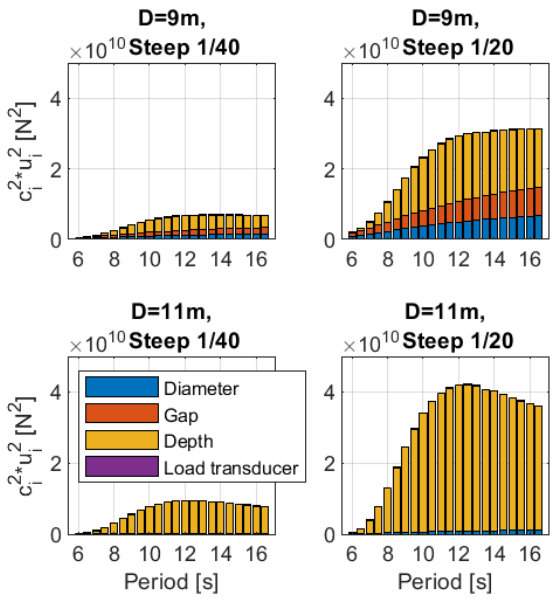

Figure 3: SQUARE OF THE STANDARD UNCERTAINTY FOR MODEL 1 (TOP ROW) AND MODEL 2 (BOTTOM ROW) FOR A WATER DEPTH OF 27m FOR TWO WAVE STEEPNESS, 1/40 (LEFT) AND 1/20 (RIGHT).

2. RESULTS AND DISCUSSIONS

2.1 Wave calibration

The majority of the wave conditions studied here are within the limits of second and third-order Stokes wave theories. Wave calibration tests without the model were performed first. Figure 4 shows different harmonics of the measured wave elevation at the wave probe next to the model from calibration tests without the model and the tests when the model is present. The amplitudes of the harmonics were extracted from the measured signal using a narrow-band filter based on the fast Fourier transform. The black lines are theoretical values. As shown, the generated waves in both tests are in good agreement, considering the influence of the model presence.

In the calculation of the wave harmonics, we considered the wave cycles from start of the tests where no reflections from the beach are present. However, for the long waves this time interval is short, and some reflections may nonetheless occur. For waves with period larger than 12s, the measurements show oscillations around the theoretical values, which may be due to reflections.

With the application of the second order correction to the wavemaker motion, the second harmonics of the wave elevation from experiment follow the theoretical curve as expected. In third harmonic, there are deviations from the theoretical values, but in general, these values are very small.

Note that the first transverse resonant periods of the tank for water depth 27 m and 33 m are 16.46 and 15.35 s, respectively. Therefore, we have influence of the tank resonant mode for large periods in the wave elevation measurements and consequently in the hydrodynamic loads.

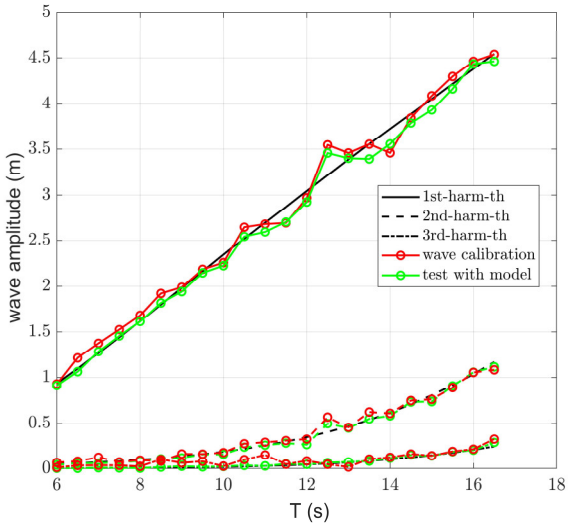

Figure 4: AMPLITUDE OF THE FIRST THREE HARMONICS OF THE WAVE ELEVATION AT THE PROBE NEXT TO THE MODEL POSITION FOR WATER DEPTH 27m AND STEEPNESS 1/30. GREEN AND RED POINTS ARE THE MEASUREMENTS FROM THE CALIBRATION TEST AND THE TEST WITH THE MODEL, RESPECTIVELY. THE BLACK LINES ARE THEORITICAL VALUES.

2.2 Measured Wave Forces

Figure 5 shows the first, second, and third harmonics of the measured forces on the monopile models. The time series of forces from experiments were band-pass filtered based on Fourier transform to obtain the different harmonics. The amplitude of the first three harmonics of the force for the two models, for two water depths and three wave steepnesses of 1/40, 1/30 and 1/22 are presented. The loads are non-dimensionalized by $\rho g a^2 A$, where ρ is the water density, g ia gravitational acceleration, a is the radius of the model, and A is the amplitude of the first harmonic of the measured calibrated waves. It must be mentioned that the model with smaller diameter was segmented and built with horizontal segments with opening between the segments. The openings represent approximately 4.5 % of the total area, and 1.8 % of the submerged volume. In the present work, the influence of changing diameter cannot be completely separated from the effects of having a segmented model.

First order near-field diffraction effects are expected to be negligible since the wavelength-to-model diameter ratio (λ/D) is large. The inertial forces are dominant in all cases; the drag forces will be small but not negligible.

Due to the negligible near-field wave diffraction, the first harmonic of the force was expected to be independent of the diameter. However, some differences can be observed, particularly for small wave periods. These differences are not completely captured by the MacCamy-Fuchs model, as shown in Section 2.3.

As Figure 5 shows, the non-dimensional second harmonic of the force is larger for the smaller diameter model in short waves. This may be due to second-order free-surface diffraction for short waves, which tend to reduce the second order force on the larger model. Tank side-wall reflections of second and third order waves might be a possible source of error. For the third harmonic, the differences between the curves of different diameters can be seen for both short and long waves in both water depths. The relative differences due to the effect of diameter are larger for the steeper waves, where the KC numbers are large, and where flow separation may become more important [8].

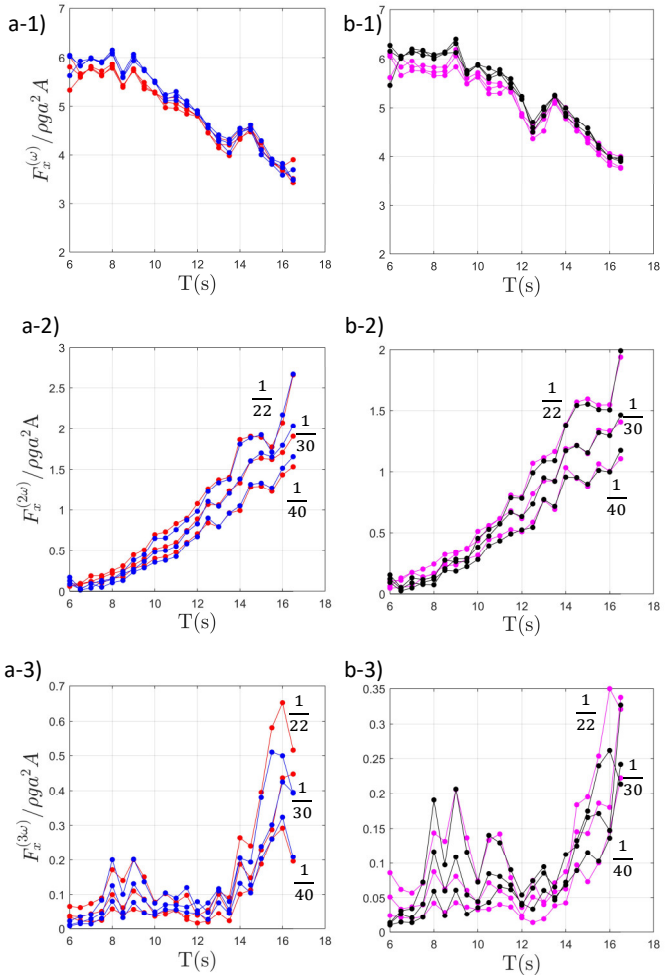

Figure 5: MEASURED AMPLITUDE OF THE FIRST THREE HARMONICS OF THE FORCE FOR THE TWO MODELS, FOR TWO WATER DEPTHS AND THREE WAVE STEEPNESSES OF 1/40, 1/30 AND 1/22. WATER DEPTH $\boldsymbol{h = 27}$ m (a) AND $\boldsymbol{h = 33}$ m (b). RED AND MAGENTA: MODEL 1, $\boldsymbol{D = 9}$ m, BLACK AND BLUE: MODEL 2, $\boldsymbol{D = 11}$ m.

In previous studies regarding the effect of the model segmentation [11], the differences between segmented and uniform model were very small for the first harmonic of the loads, however, for the higher harmonics, the influence of the segmented structure could be seen. Here since we have both effects of the diameter and segmentation, it is difficult to assess these effects separately.

The influence of changing the water depth on the force harmonics can be seen in Figure 5, where part (a) presents water depth $h = 27$ m and part (b) is for $h = 33$ m. The first harmonic of the measured force is slightly larger for larger depth for both models. However, the second and especially third harmonic force increase from the larger depth to the smaller one.

2.3 Comparisons with Calculated Results

Figure 6 and Figure 8 show the amplitude of different harmonics of the global force in different wave periods for the two models at the water depth 27 m, for two steepnesses of 1/30 and 1/22. The red points are from the measurements while the continuous lines represent calculated values based on different methods. The error bars on the first order results for the measurements are based on the expanded uncertainty described in section 1. The common version of Morison's equation can be written as:

$$dF = \rho\pi a^2 C_m \, \partial u/\partial t + \rho C_d a|u|u \qquad (2)$$

Where u is the x-component of the fluid velocity, Here, the fifth-order Stokes wave theory is used in the calculations of wave kinematics. The first term in the equation is the mass term that is proportional to the acceleration. Here with the circular cylinder model and the assumption of long wave theory, the mass coefficient, C_m, is considered to be constant and equal to 2. The second term is the quadratic drag term and the drag coefficient is $C_d = 1$. The so-called modified Morison's equation is obtained by replacing the $\partial u/\partial t$ term with the total advection term:

$$dF = \rho\pi a^2 C_m(\partial u/\partial t + u\,\partial u/\partial x + w\,\partial u/\partial z) + \rho C_d a|u|u \qquad (3)$$

The black curves in Figure 6-8, marked as Mor, correspond to the values obtained using equation (3) together with the fifth-order Stokes wave theory integrated to the instantaneous fifth-order free surface. Blue curves are the generalized FNV theory for finite depth based on Kristiansen and Faltinsen (2017) [8], referred to as KF, also using fifth order wave kinematics. The green curves, marked as KFd, are KF results with an additional drag force term, the same drag formulation as in the second term in Morison equation (2). In all calculations, the measured mean wave elevation during calibration was used as input to the numerical wave generation, hence the obtained curves are not smooth. For the first harmonic force, the magenta curve is based on the MacCamy-Fuchs (M.F.) method, i.e. the diffraction solution for a vertical cylinder.

For Model 1 ($D = 9$ m), with steepness 1/30, Figure 6 shows that the first harmonic loads from the experiments and the different calculation methods are close to each other, except that the MacCamy-Fuchs solution gives a slightly larger value of C_m (in particular for the shortest waves). The modified Morison's equation and the KF theory are almost the same for the first harmonic. The difference between these two formulations is related to the inclusion of the $u\,\partial u/\partial x$ term multiplied by C_m (modified Morison) or by 1 (KF). For larger periods, some of the differences between the measurements and the calculations for the first harmonic might also be due to the sloshing mode of the tank or reflections from the beach: these factors are not included in the simple formulation of the error bars. For shorter wave periods, uncertainties in the wave amplitude measurement might also be important.

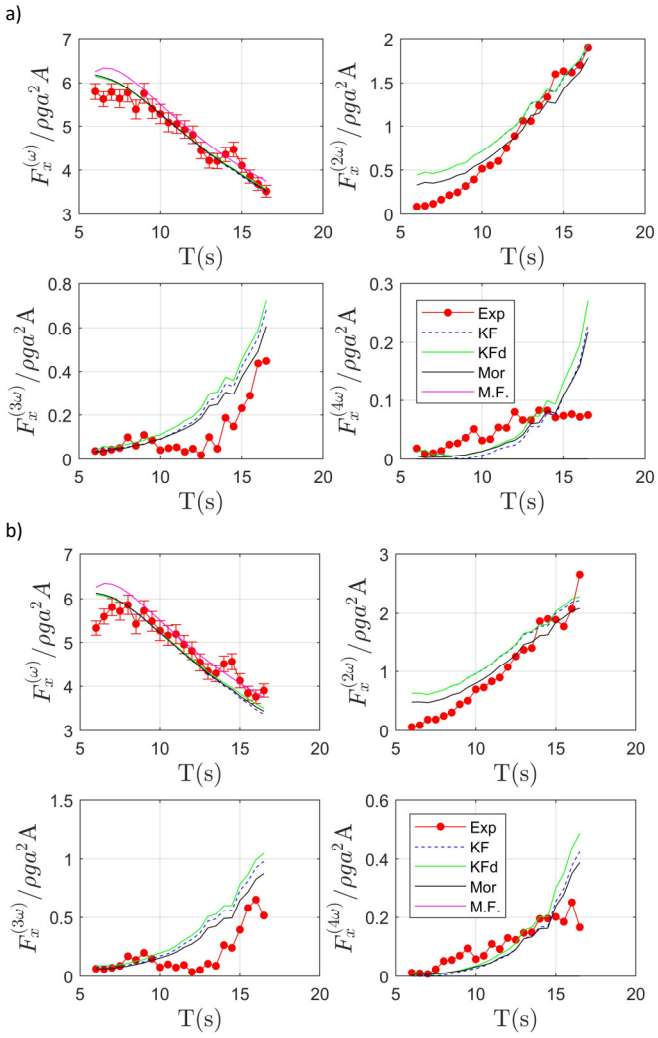

Figure 6: FIRST TO FOURTH HARMONICS OF THE SHEAR FORCE AT MUDLINE FOR MODEL 1, D=9m, WATER DEPTH 27m, STEEPNESS OF 1/30(a) AND 1/22(b).

KF and modified Morison both overpredict the global second harmonic loads in short waves, while the modified Morison gives a better prediction. The effect of the added drag term in KFd theory is negligible for the second harmonic force. For the larger periods, the calculations based on modified Morison underestimate the second harmonic. The predictions by the KF theory are closer to the measurements for the large wave periods.

The calculations give large estimations for the global third and fourth harmonics when the wave period (T) is larger than 10 s. The maximum error is about 100 % for periods smaller than 10 s, however, it becomes as large as 300 % for larger periods. The values obtained by KFd show that the additional drag term causes even more overestimation of the higher harmonics of the force.

When the steepness increases to 1/22, the first harmonic of the global force is under predicted (about 10%) by the KF and modified Morison for periods more than 10 s (Figure 6 (b)). In this case, the MacCamy-Fuchs solution agrees better with the measurements. The overprediction of the higher harmonics of the loads by the calculation methods are more pronounced for steeper waves. As expected, the amplitude of the higher harmonics of the loads is larger for the steeper

waves. For the fourth harmonic, the calculations are following the trend of measured values for steepness 1/22, though the amplitudes are not matched particularly well.

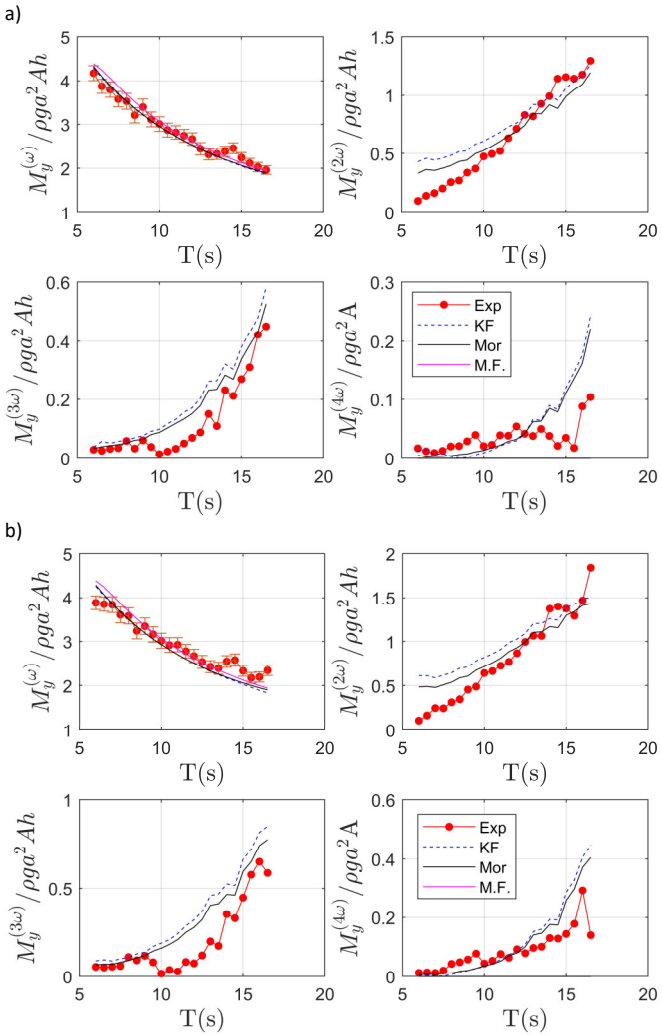

Figure 7: FIRST TO FOURTH HARMONICS OF THE MOMENT AT MUDLINE FOR MODEL 1, $\boldsymbol{D = 9}$ m, WATER DEPTH 27 m, STEEPNESS OF 1/30(a) AND 1/22(b).

Figure 7 shows the first four harmonics of the mudline moment, for Model 1 ($D = 9$ m), with steepness 1/30 and 1/22. The mudline moments are non-dimensionalized by $\rho g a^2 A h$, where a is the radius of the model, and A is the amplitude of the first harmonic of the measured calibrated waves and h is water depth. The red points are experimental measurements and the continuous lines are obtained by the calculations. Similar to the force calculations, the moment values are obtained by KF theory and modified Morison equations as well as MacCamy-Fuchs equation.

For the first harmonic moment, the experiments and different calculation methods are close to each other for steepness 1/30. For the steeper waves, KF and modified Morison underpredict the first harmonic of the moment compared to the measurements for long waves.

For the second harmonic of the moment, the trends are similar to the second harmonic of the force. For the third and fourth harmonics of the moment, for both steepnesses, the values obtained by KF and modified Morison show larger estimations compared to the measured moment.

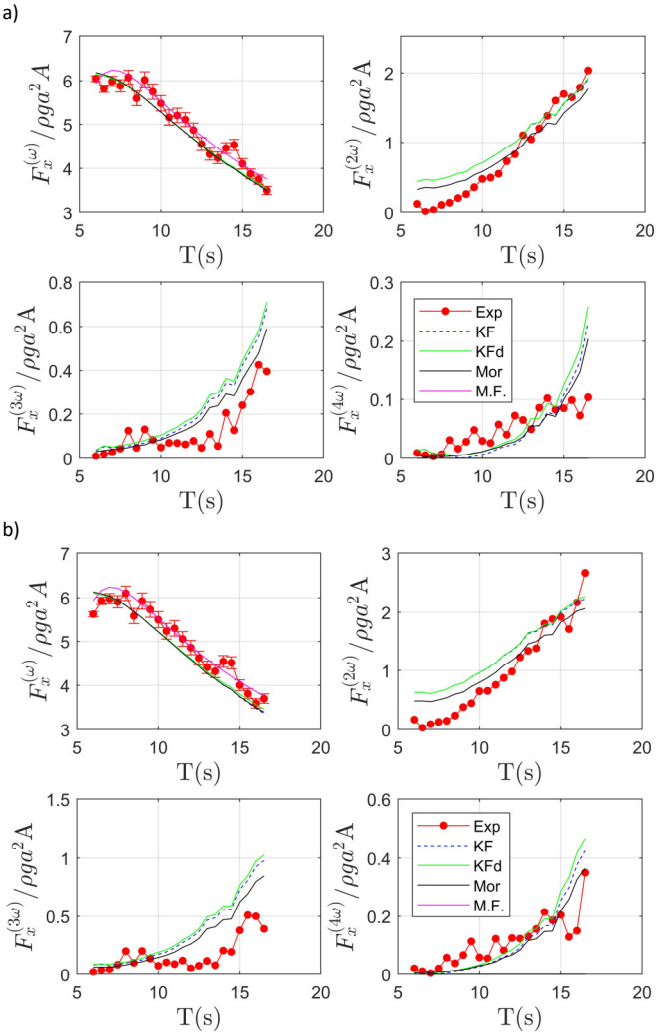

Figure 8: FIRST TO FOURTH HARMONICS OF THE SHEAR FORCE AT MUDLINE FOR MODEL 2, D=11m, WATER DEPTH 27m, STEEPNESS OF 1/30(a) AND 1/22(b).

Figure 8 shows different load harmonics for Model 2 with diameter of 11 m. For this model, similar differences between calculations and measurements are obtained. The estimated experimental error is smaller than in the $D = 9$ m case because the larger model does not have the segmentation. However, for the first harmonic for both steepnesses, MacCamy-Fuchs solution gives a better estimation for the measured forces and moments up to period 12s for the larger model.

For the second harmonic, as with the smaller diameter, all theories overpredict the forces for small periods, while values obtained by KF are close to the measurements for large periods. For the third harmonic, for periods larger than 10 s, KF and modified Morison overestimate the forces. The calculated values for the fourth harmonics of the force in the steeper wave, for large periods, are close to the measured values from experiment. The mudline moments shown in Figure 9 follow similar trends. Note that in this study mass and drag coefficients assumed to be constant and equal to 1 for all wave conditions, it is expected that a better estimation

of these parameters depending on KC and Re numbers could give a better result.

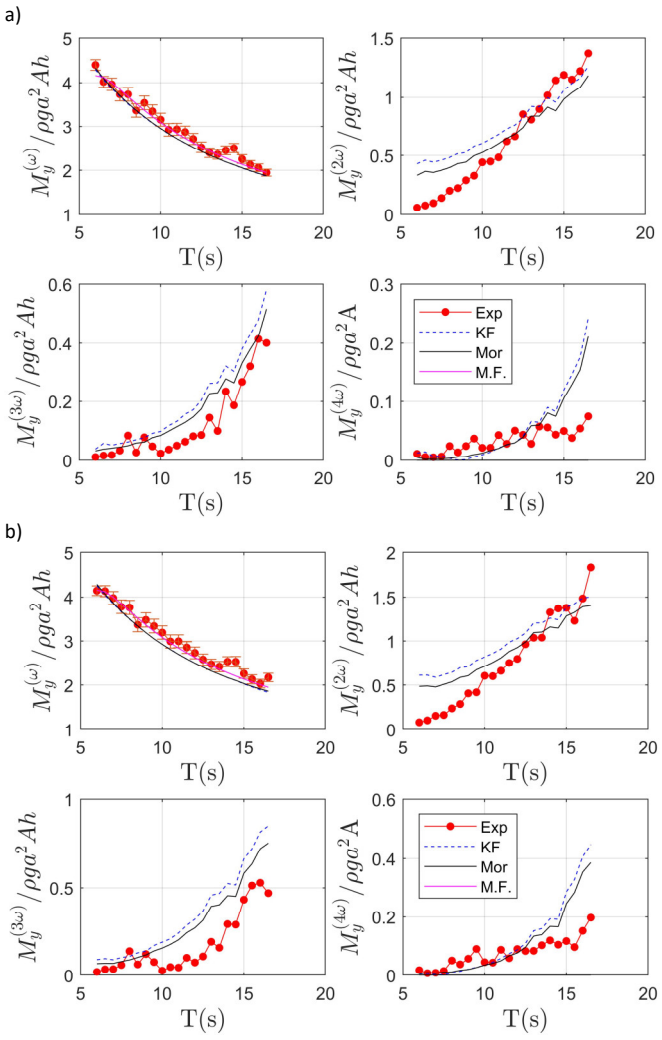

Figure 9: FIRST TO FOURTH HARMONICS OF THE MOMENT AT MUDLINE FOR MODEL 2, $\boldsymbol{D = 11}$ m, WATER DEPTH 27 m, STEEPNESS OF 1/30 (a) AND 1/22 (b).

CONCLUDING REMARKS

Validated load models for larger diameter monopile support structure for offshore wind turbines are important due to the ringing type resonant responses of the structure in the steep waves. The results from an experimental campaign at 1:50 scale for two large diameter monopiles ($D = 9$ m and $D = 11$ m) for regular waves were presented. Experimental uncertainty due to the model diameter, the water depth, the segmentation on model 1, and the load transducer at mudline for the first harmonic force and moment was estimated. The harmonics of the global force and mudline moments were compared to the calculated values based on generalized FNV theory and a modified form of Morison's equation with fifth-order wave kinematics integrated to the instantaneous fifth-order free surface. For the larger diameter (Model 2), MacCamy-Fuchs gave a better estimation of the first order force and moment especially for wave periods below 12s, due to the slight increase in the effective C_m for these combinations of wavelength and diameter. The trends in the results for higher order loads were generally consistent with the observations $D = 7$ m in [8], although the discrepancies between experimental and theoretical values for the second and third harmonic of the force and moment were somewhat larger in the present work. For the second harmonics, for the short waves, calculations overpredicted the forces while for the large waves, the opposite behavior was observed. The third harmonic of the force, which is anticipated to be most critical for ringing, was overpredicted by the calculations (similar to [8]) and the effect of having the larger diameters in the present study was minor.

ACKNOWLEDGEMENTS

The authors gratefully acknowledge the support from the Wave Loads and Soil Support for Extra-Large Monopiles (WAS-XL) project (NFR grant 268182).

REFERENCES

[1] O. Faltinsen, *Sea Loads on Ships and Offshore Structures*. Cambridge University Press, 1993.

[2] J. N. Newman, "Nonlinear Scattering of Long Waves by a Vertical Cylinder," in *Waves and Nonlinear Processes in Hydrodynamics*, J. Grue, B. Gjevik, and J. E. Weber, Eds. Dordrecht: Springer Netherlands, 1996, pp. 91–102.

[3] Š. Malenica and B. Molin, "Third-harmonic wave diffraction by a vertical cylinder," *J. Fluid Mech.*, vol. 302, pp. 203–229, Nov. 1995.

[4] Y. M. Scolan, B. Molin, G. Deleuil, and D. Martigny, "Experimental and numerical modeling of the high frequency resonant motion of a vertical cylinder in irregular waves," Dec. 1997.

[5] C. Stansberg, "Comparing ringing loads from experiments with cylinders of different diameters—an empirical study," in *BOSS '97 Conference*, 1997.

[6] O. M. Faltinsen, J. N. Newman, and T. Vinje, "Nonlinear wave loads on a slender vertical cylinder," *J. Fluid Mech.*, vol. 289, no. 1, p. 179, Apr. 1995.

[7] H. Bredmose, P. Slabiak, L. Sahlberg-Nielsen, and F. Schlütter, "Dynamic Excitation of Monopiles by Steep and Breaking Waves: Experimental and Numerical Study," in *Volume 8: Ocean Renewable Energy*, Nantes, France, 2013, p. V008T09A062.

[8] T. Kristiansen and O. M. Faltinsen, "Higher harmonic wave loads on a vertical cylinder in finite water depth," *J. Fluid Mech.*, vol. 833, pp. 773–805, Dec. 2017.

[9] "WAS XL," *WAS XL*. [Online]. Available: http://www.sintef.no/projectweb/was-xl/. [Accessed: 07-Jan-2019].

[10] L. Li, Z. Gao, and T. Moan, "Joint Environmental Data at Five European Offshore Sites for Design of Combined Wind and Wave Energy Devices," in *Volume 8: Ocean Renewable Energy*, Nantes, France, 2013, p. V008T09A006.

[11] T. Kristiansen, E. E. Bachynski, F. Bickert, A. Hniche, V. Kocher, and A. Liandrat, "Aspects in Model Testing of a Monopile in Steep Waves," in *Volume 1: Offshore*

Technology, Trondheim, Norway, 2017, p. V001T01A051.
[12] L. Suja-Thauvin, J. R. Krokstad, E. E. Bachynski, and E.-J. de Ridder, “Experimental results of a multimode monopile offshore wind turbine support structure subjected to steep and breaking irregular waves,” *Ocean Eng.*, vol. 146, pp. 339–351, Dec. 2017.
[13] “Guide to the Expression of Uncertainty in Experimental Hydrodynamics,” p. 17, 2014.